Published in final edited form as:
*Dev Cell*. 2013 September 16; 26(5): 496–510. doi:10.1016/j.devcel.2013.08.005.

# A Conserved RhoGAP Limits M-phase Contractility and Coordinates with Microtubule Asters to Restrict Active RhoA to the Cell Equator During Cytokinesis

**Esther Zanin**[1,4], **Arshad Desai**[1], **Ina Poser**[3], **Yusuke Toyoda**[3], **Cordula Andree**[3], **Claudia Moebius**[3], **Marc Bickle**[3], **Barbara Conradt**[4], **Alisa Piekny**[2], and **Karen Oegema**[1,@]

[1]Department of Cellular and Molecular Medicine, Ludwig Institute for Cancer Research, University of California, San Diego, La Jolla, CA 92093, USA

[2]Department of Biology, Concordia University, Montreal, Quebec H4B 1R6, Canada

[3]Max Planck Institute of Molecular Cell Biology and Genetics, Pfotenhauerstrasse 108, D-01307 Dresden, Germany

[4]Center for Integrated Protein Science CIPSM, Department Biology II, Ludwig-Maximilians University, Munich, 82152 Planegg-Martinsried, Germany

## SUMMARY

During animal cell cytokinesis, the spindle directs contractile ring assembly by activating RhoA in a narrow equatorial zone. Rapid GTPase activating protein (GAP)-mediated inactivation (RhoA flux) is proposed to limit RhoA zone dimensions. Testing the significance of RhoA flux has been hampered by the fact that the GAP targeting RhoA is not known. Here, we identify M-phase GAP (MP-GAP) as the primary GAP targeting RhoA during mitosis/cytokinesis. MP-GAP inhibition caused excessive RhoA activation in M-phase leading to the uncontrolled formation of large cortical protrusions and late cytokinesis failure. RhoA zone width was broadened by attenuation of the centrosomal asters but was not affected by MP-GAP inhibition alone. Simultaneous aster attenuation and MP-GAP inhibition led to RhoA accumulation around the entire cell periphery. These results identify the major GAP restraining RhoA during cell division and delineate the relative contributions of RhoA flux and centrosomal asters in controlling RhoA zone dimensions.

### Keywords

Mitosis; RhoA; Cytokinesis; MP-GAP; Ect2

## INTRODUCTION

Cytokinesis completes mitosis, partitioning the contents of a single cell into two. In animal cells, cytokinesis is accomplished by an equatorial contractile ring (Fededa and Gerlich, 2012; Green et al., 2012) whose assembly is orchestrated by the anaphase spindle-dependent

[@]Corresponding author: koegema@ucsd.edu, Phone:(858) 534-9576, Fax: (858) 534-7750, Address: CMM East Rm 3080, 9500 Gilman Dr., La Jolla, CA 92093-0653.

formation of a narrow zone of active, plasma membrane-associated RhoA (Bement et al., 2006; Piekny et al., 2005; von Dassow, 2009). Active RhoA promotes contractile ring assembly through effectors including the cytokinesis formin, which nucleates actin filaments, and Rho kinase, which recruits and activates myosin-II (Bement et al., 2006; Goode and Eck, 2007; Matsumura et al., 2011; Piekny et al., 2005). Classic micromanipulation experiments in echinoderm eggs demonstrated that moving the spindle causes furrow regression and formation of a new furrow above the spindle midplane (Rappaport, 1985). A recent rendition of this experiment with a fluorescent probe for active RhoA suggested that furrow repositioning is mediated by dynamic specification of the RhoA zone (Bement et al., 2005).

Rho family GTPases are activated by guanine nucleotide-exchange factors (GEFs), which promote exchange of GDP for GTP and target the GTPase to the membrane (Rossman et al., 2005), and are inactivated by GTPase activating proteins (GAPs) that enhance their intrinsically low hydrolysis rate (Tcherkezian and Lamarche-Vane, 2007). Specification of a narrow equatorial zone of active RhoA is proposed to involve local activation of RhoA at the cell equator coupled to two mechanisms that negatively regulate RhoA: inactivation at the cell poles by the centrosomal microtubule asters (D'Avino et al., 2005; Green et al., 2012; von Dassow, 2009) and global inactivation by a constitutive GAP activity (RhoA flux; Bement et al., 2006; Miller and Bement, 2009). The RhoA flux model predicts that reducing GAP-mediated RhoA turnover will broaden the RhoA zone due to increased diffusion of active RhoA generated by the equatorial stimulus through the membrane (Bement et al., 2006).

The broadly conserved GEF Ect2 activates RhoA to promote cell rounding (Matthews et al., 2012) and contractile ring assembly (reviewed in Fededa and Gerlich, 2012; Green et al., 2012). After chromosome segregation in anaphase, mechanisms that localize Ect2 to the central spindle are thought to preferentially activate RhoA at the cell equator (Fededa and Gerlich, 2012; Green et al., 2012) and promote its loading onto the adjacent equatorial plasma membrane (Su et al., 2011; Frenette et al., 2012). By comparison, the relative contributions of the two negative regulatory mechanisms in limiting active RhoA to a narrow equatorial zone during cytokinesis are less clear. Spindle displacement in *C. elegans* embryos (Werner et al., 2007), micromanipulation studies in grasshopper spermatocytes (Chen et al., 2008), direct imaging of myosin dynamics in vertebrate cells (Zhou and Wang, 2008) and drug or laser-based ablation of astral microtubules (Bement et al., 2005; Foe and von Dassow, 2008; Murthy and Wadsworth, 2008; von Dassow et al., 2009) have all supported the notion that centrosomal asters suppress cortical contractility/RhoA activation in their vicinity; however, the molecular basis for this suppression is not known. Similarly, testing the RhoA flux model requires identification of the major RhoA GAP during cell division, whose identity has been unclear. The GAP domain of CYK-4, a subunit of the centralspindlin complex that localizes to the central spindle, has been proposed to inactivate RhoA (Jantsch-Plunger et al., 2000), and a broader RhoA zone has been reported in *Xenopus* embryos expressing GAP-dead CYK-4 (Miller and Bement, 2009). However, work in *C. elegans* has suggested that the CYK-4 GAP domain promotes, rather than opposes, RhoA activation (Canman et al., 2008; Loria et al., 2012). In addition, the primary *in vitro* targets

of CYK-4 are Rac and Cdc42 rather than RhoA (Bastos et al., 2012; Jantsch-Plunger et al., 2000; Kawashima et al., 2000; Minoshima et al., 2003; Toure et al., 1998), and Rac inhibition partially suppresses the effects of inhibiting CYK-4 on cytokinesis (Canman et al., 2008; D'Avino et al., 2004). This prior work suggests that CYK-4 is likely not the major GAP activity countering Ect2-mediated RhoA activation during cell division. p190RhoGAP, which mediates actin cytoskeleton reorganization in response to growth factor stimulation (Chang et al., 1995), integrin engagement (Arthur and Burridge, 2001; Nakahara et al., 1998), and v-Src-mediated transformation (Fincham et al., 1999), has also been proposed to function during cytokinesis. However, while its overexpression leads to increased multinucleation in cultured vertebrate cells (Su et al., 2003; Su et al., 2009), the effects of p190RhoGAP inhibition during mitosis have not been characterized, and inhibition of the *C. elegans* p190RhoGAP homolog, *rga-5*, does not cause mitotic defects (Kamath et al., 2003; Rual et al., 2004; Sonnichsen et al., 2005).

Here, we identify the primary GAP opposing RhoA activation during mitosis and examine the roles of RhoA flux and the asters in limiting RhoA zone dimensions during cytokinesis. An analysis of candidate RhoGAPs in *C. elegans* highlighted the importance of a pair of homologous RhoA GAPs, RGA-3 and RGA-4, that were previously implicated in RhoA regulation during polarity establishment (Schmutz et al., 2007; Schonegg et al., 2007). A screen of the 67 predicted human RhoGAPs revealed a previously uncharacterized GAP whose inhibition results in hypercontractility specifically during mitosis/cytokinesis, leading us to name it M-phase GAP (MP-GAP). MP-GAP is a member of an ancient metazoan RhoA GAP family that includes *C. elegans* RGA-3/4 as distantly related orthologs. MP-GAP preferentially targets RhoA *in vitro*, and the hypercontractility induced by MP-GAP inhibition *in vivo* requires RhoA activation. In the absence of centrosomal asters, MP-GAP inhibition broadens the RhoA zone. However, in the presence of the asters, MP-GAP inhibition accelerates the accumulation of contractile ring proteins at the cell equator and promotes formation of large cortical protrusions, but does not alter RhoA zone dimensions. Thus, under normal conditions MP-GAP mediated RhoA flux constrains RhoA activation to suppress protrusion formation, but the dimensions of the equatorial RhoA zone are dominantly specified by the centrosomal asters. In addition to identifying the major RhoA GAP functioning during cell division, this effort defines the relative roles of the two negative regulatory mechanisms that shape the RhoA zone during cytokinesis.

## RESULTS

### The GAP activity of RGA-3/4, but not of CYK-4, restrains RhoA activity in the *C. elegans* embryo

Ect2 inhibition prevents RhoA activation and cortical contractility (for an example in the *C. elegans* embryo see Movie S1). We expected that inhibition of the major GAP opposing RhoA activation during cytokinesis would lead to hypercontractility, a phenotype opposite of that resulting from Ect2 inhibition (Fig. 1A). *C. elegans* has 23 predicted RhoGAPs. Prior genome-wide RNAi screens characterized 20 of these, and we analyzed the remaining three (2RSSE.1, ZK669.1, and Y34B4A.8). Of the 23 predicted Rho GAPs, only 3 were required

for embryonic viability following RNAi-mediated depletion: CYK-4, RGA-3 and RGA-4 (Fig. 1B, Table S1).

As noted above, CYK-4 is implicated in cytokinesis, but its GAP activity is more likely to target Rac and/or Cdc42 than RhoA. RGA-3/4 are homologous functionally redundant RhoA GAPs shown to inactivate RhoA during polarity establishment (Schmutz et al., 2007; Schonegg et al., 2007). Prior work on all three proteins has relied on depletions or temperature-sensitive mutations that may affect other functions in addition to GAP activity. To analyze the consequences of specifically inactivating GAP activity, we engineered catalytically inactive (GAP-Defective) mutant alleles (Rittinger et al., 1997), and determined their effects on mitosis in the one-cell embryo. We established single-copy insertion transgenic systems, expressing GFP-tagged wild-type and GD (GAP-Defective) CYK-4 or RGA-3 under the control of their endogenous regulatory sequences (Fig. 1C,D). The *cyk-4* transgene was additionally engineered to be resistant to a dsRNA targeting endogenous *cyk-4* (Fig. S1A).

As expected, depletion of endogenous CYK-4 in the absence of a transgene resulted in embryonic lethality and cytokinesis failure in the first division with partial cleavage furrow ingression followed by regression. These phenotypes were rescued by wild-type CYK-4::GFP but not CYK-4$^{GD}$::GFP (Fig. 1E,F; Movie S2) even though both were expressed at similar levels (Fig. 1C) and localized to the spindle midzone (data not shown). Thus, inhibiting the GAP activity of CYK-4 results in decreased contractility, rather than the hypercontractility expected to result from a catalytically-defective major RhoA GAP.

Next, we analyzed the requirement for RGA-3/4 GAP activity. A double deletion of *rga-3* and *rga-4* (Fig. S1B) was maternal effect embryonic lethal. Homozygous *rga-3*Δ *rga-4*Δ adults lay embryos lacking maternally loaded protein (referred to as *rga-3/4*Δ embryos) that are inviable (Fig. 1F). The cortex in *rga-3/4*Δ embryos is dramatically hypercontractile and 36% of embryos fail the first cytokinesis (Fig. 1E,F). This hypercontractility was suppressed by inhibiting RhoA activation using ECT-2 depletion (Fig. S1C). Embryonic lethality, hypercontractility, and first cytokinesis failure in *rga-3/4*Δ embryos were all rescued by wild-type GFP::RGA-3 but not GFP::RGA-3$^{GD}$ (Fig. 1E,F; Movie S3) even though both proteins were expressed at comparable levels (Fig. 1D). Thus, RGA-3/4 GAP activity is essential to prevent hypercontractility during mitosis in the early *C. elegans* embryo.

RGA-3/4 localized to the cortex and the centrosomal region during mitosis and cytokinesis (Fig. 1G, Fig. S1D,E), as it does during embryo polarization (Schonegg et al., 2007), and this localization depended on RhoA (RHO-1 in *C. elegans*; Fig. 1G) and the RhoA GEF ECT-2 (Fig. S1D), but not on CDC-42 or Rac (CED-10; data not shown). Although mutating the arginine finger abolishes the ability of the GAP domain to promote GTP hydrolysis, it does not prevent binding of the GAP domain to its target GTPase (Ahmadian et al., 1997; Graham et al., 1999; Leonard et al., 1998). Consistent with this, GFP::RGA-3$^{GD}$ was strongly enriched on the cortex compared to wild-type GFP::RGA-3 (Fig. 1H, Fig. S1F; GFP::RGA-3$^{GD}$ accumulates asymmetrically on the anterior cortex due to embryo polarity) and this localization depended on RHO-1 and the ECT-2 GEF (Fig. 1H; S1G), but not on Cdc42 (Fig. 1H, *cdc-42(RNAi)*) or Rac (Fig. 1H, *ced-10 & rac-2(RNAi)*).

The RhoA-dependent cortical accumulation of GAP-Defective RGA-3/4 provides strong *in vivo* evidence that RGA-3/4 GAP activity specifically targets RhoA. We conclude that the GAP activity of RGA-3/4 but not of CYK-4 counters RhoA activation during the early embryonic divisions of *C. elegans*.

## Identification of a conserved M-Phase GAP (MP-GAP) family that controls cortical contractility during mitosis and cytokinesis

Sequence searches with RGA-3/4 failed to identify highly related orthologs outside of nematodes other than highlighting the presence of a RhoGAP domain. To identify human GAPs that control RhoA activity during mitosis and cytokinesis, we therefore took an unbiased screening approach. To define the phenotypic fingerprint of excessive RhoA activation during mitosis and cytokinesis, we first generated isogenic HeLa cell lines expressing wild type or constitutively active GFP::RhoA ($RhoA^{Q63L}$) under the control of an inducible promoter. In contrast to mitotic cells expressing wild-type GFP::RhoA, nearly all mitotic cells expressing constitutive active GFP::$RhoA^{Q63L}$ formed large cortical protrusions (Fig. 2A,B). Approximately 20% of cells expressing GFP::$RhoA^{Q63L}$ also failed cytokinesis (Fig. 2C). These results suggested that protrusion formation is a hallmark of excessive RhoA activation in mitotic cells.

We next targeted each of the 67 known human Rho GAPs with four independent siRNA oligos and quantified the percentage of mitotic cells with large protrusions. Three genes with known roles in mitosis (Kif11 (Eg5), PLK1 and MKLP1) were also included in the screen to control for the efficacy of the siRNA procedure. Cells were fixed and stained for DNA and RhoA and image stacks were acquired for multiple fields per well using a high content imaging system. The assay was performed three times and the mean mitotic cells analyzed per gene was 43 (range 23–77). In this screen, inhibition of only one previously uncharacterized human GAP, ARHGAP11A, led to a significant increase in protrusion formation (Fig. 2D,F).

ARHGAP11A has a domain structure similar to RGA-3/4, with an N-terminal GAP domain in the context of a larger protein lacking other functional motifs (Fig. 2E). This architecture is present in only three (ARHGAP11A, FAM13A and FAM13B) of the 67 predicted human RhoGAPs. To determine if there is any redundancy between the 3 N-terminal GAP domain RhoGAPs, we analyzed protrusion formation after depleting FAM13A and FAM13B individually and in combination with each other and ARHGAP11A (Fig. 2F, S2E). Co-depletion of FAM13A, FAM13B or both along with ARHGAP11A did not enhance the ARHGAP11A phenotype (Fig. S2E), suggesting that only ARHGAP11A plays a significant role in limiting protrusion formation in mitotic cells.

Humans, but not other primates, have a second homologous gene ~2Mb away from *ARHGAP11A*, called *ARHGAP11B*, which is likely derived from a local duplication on chromosome 15 (Riley et al., 2002). The *ARHGAP11B* locus directs expression of a truncated 267 aa protein homologous to the ARHGAP11A GAP domain (Fig. S2A,B). Our siRNA is outside the region conserved between the two genes and targets only ARHGAP11A (Fig. S2C). These results suggest that ARHGAP11A is the critical Rho GAP that counters RhoA activation during mitosis in human cells. Based on the phenotypic

analysis described below we decided to name ARHGAP11A, MP-GAP for M-Phase GAP. Blast searches and sequence alignments based on the GAP domain (Fig. 2G), revealed MP-GAP homologs in vertebrates, insects (but not in *Drosophila*), the sea anemone (phylum *Cnidaria*) and the primitive metazoan *Trichoplax* adherens (phylum Placozoa); *C. elegans* RGA-3/4 appear to be evolutionarily distant members of the ancient MP-GAP family (Fig. 2G, Fig. S2D).

We next analyzed MP-GAP localization by engineering a HeLa cell line expressing MP-GAP::GFP from an integrated BAC (in parallel, we tested two commercial antibodies but neither worked for immunofluorescence or immunoblotting). MP-GAP::GFP was enriched on the cortex from prophase through anaphase and concentrated in the nucleus from late telophase through interphase (Fig. 3A). The MP-GAP::GFP cell line also enabled identification of a single siRNA oligo that efficiently reduced protein levels by >95% (Fig. 3B).

Consistent with its sequestration in the nucleus, the morphology of interphase cells appeared normal following MP-GAP depletion (Fig. S3A). To confirm this observation, we generated a HeLa cell line expressing Anillin::GFP from an integrated BAC, and performed timelapse imaging. When Anillin::GFP was in the nucleus during interphase, the morphology of MP-GAP siRNA cells was indistinguishable from controls (Fig. 3C,D). The timing of mitotic events was also similar in control and MP-GAP siRNA treated cells (Fig. S3B,C). However, MP-GAP-depleted cells began to form large cortical protrusions concomitant with mitotic cell rounding. Protrusions were at least 2–3 fold bigger than blebs in control anaphase cells, were more stable than blebs, had a narrow opening to the cell body, were enriched for cortical Anillin::GFP (Fig. 3C) and filamentous actin (Fig. S3D), and were present throughout mitosis and cytokinesis (Fig. 3C,D; Movies S4, S5). Quantification of the spatial distribution of protrusions in fixed early anaphase cells did not reveal a spatial bias for their formation on the equatorial versus polar cortex (Fig. 3E).

Next we determined whether MP-GAP inhibition affected Ect2 localization by monitoring Ect2::GFP expressed from an integrated BAC. Ect2::GFP localized to the spindle midzone and the equatorial plasma membrane during anaphase and cytokinesis in a similar fashion in control and MP-GAP depleted cells (Fig. 3F), suggesting that MP-GAP inhibition leads to protrusion formation by failing to inactivate RhoA rather than altering the pattern of RhoA activation.

We next monitored cytokinesis following MP-GAP inhibition in two different HeLa cell lines (Fig. 3G). In HeLa cells expressing a GFP tagged plasma membrane marker, cytokinesis never failed following treatment with control siRNA, but failed 18% of the time when MP-GAP was depleted. In most cases (15%), this was a late failure, with the furrow regressing ~90 minutes after anaphase onset (Fig. 3G); however, a small percentage of cells (3%) exhibited an early failure in which they failed to form a cleavage furrow. HeLa cells expressing Ect2::GFP were sensitized to early failure, potentially due to excess RhoA activation; ~5% exhibited early failure when treated with control siRNA and this was increased to 17% following treatment with MP-GAP siRNA. Cumulatively, these results suggest that MP-GAP inhibited cells are prone to cytokinesis failure. In a non-sensitized

background, the majority of MP-GAP inhibited cells assemble a contractile ring that constricts, but at an appreciable frequency cells fail to complete abscission. In a sensitized background, the rate of early failure is substantial. We conclude that MP-GAP suppresses the formation of cortical protrusions during mitosis and cytokinesis and is required to ensure successful cytokinesis.

### MP-GAP Suppresses Cortical Hypercontractility by Targeting RhoA

To determine how MP-GAP controls cortical contractility in mitotic cells, we first tested the role of its GAP activity by using Flp-mediated recombination to generate HeLa cell lines with single copy, tetracycline-inducible, siRNA-resistant transgenes expressing GFP::MP-GAP or an equivalent GAP-Defective version. Both proteins were expressed at similar levels (Fig. 4A) and localized to the cortex (Fig. 4B). Expression of wild-type, but not GAP-Defective MP-GAP, suppressed protrusion formation during mitosis resulting from depletion of endogenous MP-GAP (Fig. 4B). Thus, the ability of MP-GAP to prevent cortical hypercontractility during mitosis requires its GAP activity.

MP-GAP is predicted to target a Rho family GTPase. To determine whether it targets RhoA, Rac1 or Cdc42 we purified the GAP domain of MP-GAP from *E. coli* (Fig. 4C) and analyzed its activity *in vitro*. In an assay monitoring phosphate generated by GTP hydrolysis, the purified MP-GAP GAP domain showed high activity towards RhoA compared to Cdc42 or Rac1 (Fig. 4C). Consistent with this *in vitro* finding, staining of fixed cells for DNA and RhoA revealed that metaphase cells depleted of MP-GAP had higher levels of RhoA at the cell cortex than control cells (Fig. 4D).

If MP-GAP targets RhoA, as suggested by the *in vitro* analysis and measurements of cortical RhoA levels, the protrusions observed following its inhibition should be suppressed by reducing RhoA activation. To test this prediction, we analyzed protrusion formation following three different perturbations expected to prevent RhoA activation: treatment with C3 exoenzyme (Fig. 4E, S4A), depletion of the Ect2 GEF (Fig. 4F, Fig. S4B), and inhibition of Plk1 with the inhibitor BI2536 (Fig. 4G, Fig. S4D). Previous work has shown that Plk1 is required for RhoA activation and contractile ring assembly (Fig. S4C; Brennan et al., 2007; Burkard et al., 2009; Burkard et al., 2007; Petronczki et al., 2007; Wolfe et al., 2009). All three treatments suppressed protrusion formation in MP-GAP depleted cells (Fig. 4E–G) and prevented contractile ring assembly in both control and MP-GAP depleted cells. Interestingly, treatment with the Rho kinase inhibitor Y27632 (Fig. 4H, Fig. S4E) suppressed protrusion formation without blocking contractile ring assembly. Staining with an antibody to phosphorylated myosin light chain (P-MLC) revealed that, in addition to enrichment in the contractile ring, P-MLC was concentrated at the base of the protrusions in MP-GAP inhibited cells (Fig. S4F). A requirement for myosin phosphorylation in protrusion formation may underlie the potent suppression observed following inhibition of Rho kinase. Taken together, the *in vitro* and *in vivo* data support the conclusion that MP-GAP suppresses protrusion formation in mitotic cells by promoting RhoA GTP hydrolysis.

## MP-GAP Inhibition Accelerates RhoA Accumulation But Does Not Alter RhoA Zone Dimensions

We next tested the consequence of inhibiting MP-GAP on the dimensions of the equatorial RhoA zone. In the RhoA flux model, reducing GAP-mediated RhoA turnover is predicted to broaden the RhoA zone (Fig. 5A; Bement et al., 2006). The RhoA zone can be monitored in fixed cells by staining for RhoA (Yonemura et al., 2004). In living cells, the RhoA zone can be indirectly monitored by following the recruitment of Anillin, which binds to and co-localizes with active RhoA (Piekny and Glotzer, 2008).

We first used timelapse imaging to monitor the dynamics of Anillin::GFP recruitment (Fig. 5B). Zone width was measured at cytokinesis onset (when the first bending of the cortex was evident, ~9 minutes after anaphase onset) by generating a scan of Anillin::GFP fluorescence intensity along a 5 pixel-wide line that encompassed the cortex from pole to pole (excluding blebs and protrusions). This analysis revealed that the width of the Anillin::GFP zone was not significantly different between control and MP-GAP siRNA treated cells ($p=0.20$; Fig. 5C). To analyze the timing of Anillin zone formation, we measured the mean Anillin::GFP fluorescence intensity over the central region of the cell (from −4 to +4 μm from the cell center) at 3, 6 and 9 minutes after anaphase onset (Fig. 5D). In control cells, Anillin::GFP was first detected at the cell equator 6 minutes after anaphase onset. By contrast, in MP-GAP siRNA treated cells, accumulation was evident by 3 minutes after anaphase onset and Anillin::GFP had accumulated to a significantly greater extent at the 6 minute timepoint than in controls (Fig. 5D). Thus, while zone dimensions were unchanged, Anillin recruitment was accelerated following MP-GAP inhibition.

To analyze RhoA directly in the absence of excessive cortical contractility, we next measured the width of the RhoA zone in synchronized, fixed HeLa cells that were treated with Blebbistatin to inhibit myosin-II mediated cortical contractility (Fig. 5E; Straight et al., 2003). The measurements were performed on early anaphase cells that had either no cleavage furrow (blebbistatin-treated and DMSO-treated control) or a slight bend to the cortex (DMSO-treated control). Although, the RhoA zone was slightly wider in blebbistatin-treated cells than in DMSO treated controls, RhoA zone dimensions were not significantly different between control and MP-GAP depleted cells for either condition (Fig. 5F; DMSO $p=0.67$, blebbistatin $p=0.37$). Treatment of cells with Blebbistatin reduced the size and number of protrusions in MP-GAP inhibited cells, but did not completely eliminate them (Fig. 5F). This is likely because blebbistatin was added at a time when numerous protrusions were already present; consistent with this, treatment of unsynchronized MP-GAP depleted HeLa cells with Blebbistatin for 1h completely blocked protrusion formation (not shown). We conclude that modulating RhoA flux by inhibiting MP-GAP accelerates Anillin accumulation at the cell equator but does not affect the spatial dimensions of the RhoA or Anillin zones.

## RhoA Zone Dimensions are Dominantly Specified by the Centrosomal Microtubule Asters

The results above indicate that inhibiting MP-GAP-mediated RhoA flux enhances RhoA activation, leads to numerous large protrusions, and accelerates RhoA accumulation at the cell equator, but surprisingly does not alter contractile ring-associated RhoA zone

dimensions. Thus, rather than being limited by RhoA diffusion, RhoA zone dimensions must be matched to the dimensions of the spindle by another mechanism. A likely possibility based on prior work is that the centrosomal asters specify RhoA zone dimensions by preventing the accumulation of active RhoA and/or contractile ring proteins in their vicinity; this mechanism must be sufficiently robust to overcome enhanced RhoA activation. This model predicts that inhibiting assembly of centrosomal microtubules should lead to a broader RhoA zone, whereas enhancing the assembly of astral microtubules should have the opposite effect, narrowing the zone of RhoA and contractile ring protein accumulation. Prior work in sea urchin embryos and porcine epithelial cells has shown that eliminating dynamic astral microtubules results in a broader zone of active RhoA (Bement et al., 2005; Foe and von Dassow, 2008; Murthy and Wadsworth, 2008; von Dassow et al., 2009). We confirmed that this was also true in HeLa cells following treatment with a low dose (10nM) of nocodazole for 10 minutes during anaphase. This treatment disrupted astral microtubules, and led to a ~30% reduction spindle midzone length, but preserved the microtubule bundles in the central spindle (Fig. 6A–C). Notably, disruption of the astral microtubules led to a 1.5 to 2 fold increase in the mean width of the RhoA and Anillin zones (Fig. 6E,F).

Since eliminating the centrosomal asters is a severe perturbation with the potential to alter RhoA regulation via ectopic means, for example by releasing microtubule-bound GEF-H1 (Chang et al., 2008), we also examined the effects on the RhoA zone of augmenting the asters via MCAK inhibition. MCAK is a kinesin that inhibits microtubule assembly (Desai et al., 1999). Treatment of cells with MCAK siRNA has previously been shown to result in longer astral microtubules (Rankin and Wordeman, 2010). MCAK siRNA did not disrupt midzone assembly or Plk1 recruitment to the central spindle (Fig. 6A) and spindle midzone dimensions in MCAK siRNA-treated cells were not significantly different from controls (Fig. 6B,C; $p=0.9$). However, MCAK inhibition led to a modest but significant ($p<0.001$) reduction in the width of both the RhoA and Anilin zones compared to controls. Quantification of total fluorescence intensity in the RhoA and Anillin zones also revealed that both were significantly reduced by MCAK inhibition ($p<0.0001$, Fig. S5), whereas total RhoA and Anillin in low dose nocodazole-treated cells were not significantly different from controls (RhoA $p=0.52$, Anillin $p=0.06$, Fig. S5). We conclude that the dimensions of the equatorial RhoA zone, while not altered by the MP-GAP inhibition-induced increase in active RhoA, can be increased or decreased by eliminating or augmenting the centrosomal asters, respectively.

We next tested whether MP-GAP mediated RhoA flux controls RhoA zone dimensions in the absence of the asters. Control and MP-GAP inhibited cells expressing Anillin::GFP were imaged starting at metaphase and nocodazole was added immediately after the cells entered anaphase (2–3 minutes after the last metaphase frame). Consistent with the results in fixed cells, eliminating the asters by nocodazole addition broadened the Anillin::GFP zone (Fig. 6G–I). When asters were attenuated in MP-GAP inhibited cells, the Anillin::GFP zone was broadened even further, with Anillin::GFP accumulating around the entire periphery of the cell (Fig. 6 G–I). These results indicate that MP-GAP mediated flux is essential to limit the RhoA zone to the cell equator when the aster-based restriction mechanism is compromised. In the absence of the two independent mechanisms that limit RhoA accumulation to the cell equator, Anillin::GFP accumulated uniformly on the cortex. However, when present, the

asters dominantly specify the RhoA zone dimension, rendering it insensitive to fluctuations in the level of RhoA activation.

## DISCUSSION

Both GAP-mediated RhoA flux (Bement et al., 2006; Miller and Bement, 2009) and inhibitory signals from the centrosomal asters (Bement et al., 2005; Foe and von Dassow, 2008; Murthy and Wadsworth, 2008; von Dassow et al., 2009) are proposed to limit the dimensions of the equatorial RhoA zone. Investigation of how these two mechanisms are integrated was limited by the fact that the primary GAP opposing RhoA activation during cell division was not known. Here, we identify MP-GAP, a member of an ancient metazoan RhoGAP family, as a key regulator of RhoA during cell division.

MP-GAP limits RhoA activity throughout mitosis to stabilize the cortex and prevent the formation of large protrusions. In the absence of the centrosomal microtubule asters, MP-GAP also restricts RhoA zone dimensions as predicted by the RhoA flux model. However, in the presence of the centrosomal asters, the dimensions of the equatorial RhoA are not affected by MP-GAP inhibition (summarized in Fig. 7). These results suggest that when present, the centrosomal asters dominantly control RhoA zone dimensions. Previous work has shown that eliminating dynamic astral microtubules leads to a broader zone of active RhoA and contractile ring protein accumulation (Bement et al., 2005; Foe and von Dassow, 2008; Murthy and Wadsworth, 2008; von Dassow et al., 2009). As eliminating centrosomal asters could upregulate RhoA via ectopic means, such as release of a microtubule-bound RhoA activator (Chang et al., 2008), we also show here that augmenting centrosomal asters by RNAi of the microtubule disassembly enzyme MCAK (Desai et al., 1999; Rankin and Wordeman, 2010) has the opposite effect. Although the molecular basis for the control of RhoA zone by the asters is not known, the fact that RhoA zone dimensions are not affected by MP-GAP inhibition suggests that the aster-based mechanism does not involve activating MP-GAP in a spatially patterned fashion.

Rather than leading to a change in RhoA zone dimensions as measured along the length of the spindle, compromising RhoA inactivation by inhibiting MP-GAP leads to the dynamic formation of large ectopic protrusions, a phenotype similar to that resulting from expression of constitutively active RhoA. We propose that MP-GAP opposes RhoA activation wherever it occurs. At the cell equator, MP-GAP slows but does not prevent RhoA activation, likely because active RhoA at the cell equator is maintained by persistent Ect2 GEF activity resulting from the proximity of the central spindle. Nascent protrusions located anywhere on the cell surface, have a narrow base and loop out away from the cell body; thus, the cortex within protrusions would presumably not be directly subject to either aster-based inhibition or to persistent Ect2 GEF signaling. Nascent protrusions would normally be terminated by MP-GAP, which would inactivate GTP-bound RhoA that is not being actively replenished. In the absence of MP-GAP, active RhoA that diffused in from other parts of the cortex would not be inactivated and protrusion geometry would protect the extruded cortex from aster-based inhibition. This could initiate the accumulation of contractile ring proteins that in turn, via positive feedback, would further promote RhoA activation. Despite the fact that aster-based inhibition maintains the general pattern of RhoA activation along the spindle,

MP-GAP inhibition results in a significant level (~20%) of cytokinesis failure, largely due to failure of abscission rather than contractile ring assembly or constriction. A role for MP-GAP-mediated downregulation of RhoA in faciliating abscission is plausible, since RhoA localizes to the midbody ring (Gai et al., 2011; Hu et al., 2012) and, along with anillin, concentrates at the sites on either side of the midbody where ESCRT-mediated cleavage occurs (Hu et al., 2012).

Our results suggest a “dominant suppression” model in which RhoA activation and diffusion are dominantly suppressed outside of a specified equatorial zone (Fig. 7). Dominant suppression by the asters would have significant advantages over zone specification through a flux-based mechanism. First, it would make the cell relatively insensitive to the precise localization of the signal activating RhoA. This could explain for example, why displacing the RhoA GEF Ect2 from its location on the central spindle does not have a dramatic effect on cytokinesis (Chalamalasetty et al., 2006). Dominant suppression would also allow rapid achievement of the state observed *in vivo*, where the profile of active RhoA resembles a step function with little to no active RhoA at the cell poles and maximal activation within an equatorial region. Feedback, in which the assembly of contractile ring proteins such as Anillin promotes RhoA activation (Piekny and Glotzer, 2008; Frennete et al., 2012), could also contribute to the rapid, step-like accumulation of contractile ring proteins within a central zone.

In summary, identification of the MP-GAP family that opposes RhoA activation during cell division has enabled comparison of the relative contribution of RhoA flux versus centrosomal asters to patterning of the active RhoA zone. Our results highlight the importance in future work of elucidating the molecular basis of the aster-based mechanism that constrains active RhoA to the cell equator.

## EXPERIMENTAL PROCEDURES

### *C. elegans* Strains and RNAi

*C. elegans* strains and dsRNAs are listed in Supplementary Experimental Procedures. Strains containing integrated *cyk-4* and *rga-3* transgenes were generated as described (Frokjaer-Jensen et al., 2008). L4 hermaphrodites were injected with dsRNA and incubated at 20°C for 20–28 h before dissection and embryo imaging. For embryo lethality tests, worms were singled 23–27 h post injection and allowed to lay embryos for 24h at 20°C. Adult worms were removed and hatched/inviable embryo were counted 24 h later.

### Microscopy, Immunofluorescence, and Image Analysis

For details on microscopy and immunofluorescence, see Supplementary Experimental Procedures. Anillin::GFP accumulation (Fig. 5D) was analyzed 3, 6 and 9 minutes after the last metaphase frame (t=0 min) in the central confocal plane in which the cell was in best focus by drawing a 5 pixel-wide linescan encompassing the pole-pole cortex (excluding blebs and protrusions). Mean cytoplasmic fluorescence intensity measured near the cell center was subtracted and the mean Anillin::GFP fluorescence intensity in the 8 μm wide region centered around the fluorescence peak calculated. All values were normalized using

the mean fluorescence intensity of control cells at 9 minutes. Anillin::GFP zone width (Fig. 5C) was measured using cortical pole-to-pole linescans when the first bending of the cortex occurs (~9 minutes after anaphase onset); zone width was measured at half maximum fluorescence intensity. Anillin and RhoA zone widths in fixed anaphase cells were similarly measured using 8 pixel-wide pole-to-pole cortical linescans. In Fig. 6I, average metaphase cortical Anillin::GFP fluorescence intensity was subtracted from cortical linescans performed 13.5 minutes after anaphase onset; values were normalized by dividing by the average fluorescence intensity between 40–50% of cell length in control cells and two linescans per cell were averaged. Anillin::GFP zone width in live cells was ~2-fold larger than RhoA/Anillin zone width in fixed cells. This difference is explained by larger size of Anillin::GFP HeLa cells and is consistent with RhoA zones scaling with cell size (Bement et al., 2005).

## HeLa Cell Lines

All cell lines are listed in Supplementary Experimental Procedures. H2B-mRFP (Histone) and MyrPalm-mEGFP (Membrane) HeLa cells were obtained from Daniel Gerlich (Steigemann et al., 2009). BAC-integrated mouse Anillin::FLAP and human MP-GAP::LAP HeLa lines were generated using BACs RP11-106G20 and RP23-73C5 (http://bacpac.chori.org) harboring human ARHGAP11A and mouse ANLN, respectively. Tagging LAP (EGFP-IRES-Neo) and FLAP (EGFP-FLAG-IRES-Neo) cassettes were PCR amplified using primers with 50 nucleotide homology. Recombineering and stable BAC transfection were performed as described (Poser et al., 2008). Clonal lines were obtained by fluorescence-activated cell sorting (FACS). Stable isogenic HeLa lines expressing GFP::MP-GAP, GFP::MP-GAP$^{GD}$, GFP::RhoA and GFP::RhoA$^{Q63L}$ were generated by FRT/Flp-mediated recombination (Gassmann et al., 2010; Tighe et al., 2004). RNAi resistance was conferred using four silent mutations in MP-GAP (attacaggcAgcTgtGgtG, changes in capital letters). Human MP-GAP and RhoA cDNA, as well as MP-GAP$^{GD}$ or RhoA$^{Q63L}$ variants were cloned into pcDNA5/FRT/TO (Invitrogen) modified to contain an N-terminal Myc-LAP epitope tag (Cheeseman and Desai, 2005; Gassmann et al., 2010). Vectors were co-transfected in HeLa Flp-In T-Rex cells with pOG44 encoding the Flp recombinase using X-tremeGENE 9 (Roche). After selection with hygromycin, colonies were pooled and transgene expression induced with 0.2 μg/mL tetracycline.

Cell culture and siRNA transfection are described in the Supplemental Experimental Procedures. Cells were fixed and stained or collected for immunoblotting 48h and 72h after transfection. Live-cell imaging was initiated 48 h after transfection. Expression of GFP::MP-GAP and GFP::MP-GAP$^{GD}$ was induced with 0.2 μg/mL tetracycline 24h after siRNA transfection and cells were fixed 24 h later. Expression of GFP::RhoA and GFP::RhoA$^{Q63L}$ was induced 16 h before imaging. MCAK siRNA cells (Rankin and Wordeman, 2010) were fixed 30 h after transfection. Nocodazole (Sigma-Aldrich) was used at a final concentration of 10nM. Unsynchronized HeLa cells were treated with nocodazole or DMSO (control) for 10 minutes prior to fixation. In Fig 6G–I, HeLa cells expressing Anillin::GFP were transfected with MP-GAP siRNA for 48h and nocodazole added 2–3 minutes after the last metaphase frame.

### Human RhoGAP siRNA screen

Hela cells were seeded in 384-well plates (Aurora, FluidX) at a density of 500 cells/well. 24 h after seeding, a Freedom Evo 200 liquid handling station (Tecan) and OligofectAMINE (Life Technologies) were used to transfect cells with 10nM stealth siRNAs (Life Technologies). 72h after transfection, cells were fixed and stained using a plate washer (EL406, BioTek and Powerwasher PW384, Tecan). 9-plane z-stacks (1.3μm intervals) were acquired for seven fields per well using an OPERA imaging system (Perkin Elmer) equipped with a 40x water-immersion objective (NA=0.9).

### *In vitro* GAP Assay

6xHis tagged MP-GAP GAP domain (1-253aa) was cloned into pET28 and expressed in BL21 *E. coli*. The GAP domain was purified (Supplementary Experimental Procedures), stored in 10% sucrose at −80°C, and dialyzed into 50mM Tris, 150 mM NaCl, 1mM $MgCl_2$ prior to the analysis with RhoGAP assay Biochem kit (BK105, Cytoskeleton, Inc.).

## Supplementary Material

Refer to Web version on PubMed Central for supplementary material.

## Acknowledgments

We thank D. Gerlich for the H2B-mRFP and MyrPalm-mEGFP expressing HeLa cell line, Y. Kohara for gene-specific cDNAs and the *Caenorhabditis* Genetics Center (P40 OD010440) for strains. K.O. and A.D. receive salary and additional support from the Ludwig Institute for Cancer Research. E.Z. was supported by a fellowship from the Deutsche Forschungsgemeinschaft (DFG, ZA 619/1-1). A.P. is supported by a grant from CIHR and B.C. is supported by grants from the National Institutes of Health (GM069950, GM076651).

## ABBREVIATIONS LIST

| | |
|---|---|
| **DIC** | differential interference contrast |
| **GAP** | GTPase Activating Protein |
| **GD** | GAP-Defective |
| **GEF** | Guanine nucleotide exchange factor |
| **MP-GAP** | M-Phase GAP |
| **NEBD** | nuclear envelope breakdown |
| **SD** | standard deviation |
| **SEM** | standard error of the mean |

## References

Ahmadian MR, Stege P, Scheffzek K, Wittinghofer A. Confirmation of the arginine-finger hypothesis for the GAP-stimulated GTP-hydrolysis reaction of Ras. Nat Struct Biol. 1997; 4:686–689. [PubMed: 9302992]

Arthur WT, Burridge K. RhoA inactivation by p190RhoGAP regulates cell spreading and migration by promoting membrane protrusion and polarity. Mol Biol Cell. 2001; 12:2711–2720. [PubMed: 11553710]

Bastos RN, Penate X, Bates M, Hammond D, Barr FA. CYK4 inhibits Rac1-dependent PAK1 and ARHGEF7 effector pathways during cytokinesis. J Cell Biol. 2012; 198:865–880. [PubMed: 22945935]

Bement WM, Benink HA, von Dassow G. A microtubule-dependent zone of active RhoA during cleavage plane specification. J Cell Biol. 2005; 170:91–101. [PubMed: 15998801]

Bement WM, Miller AL, von Dassow G. Rho GTPase activity zones and transient contractile arrays. Bioessays. 2006; 28:983–993. [PubMed: 16998826]

Brennan IM, Peters U, Kapoor TM, Straight AF. Polo-like kinase controls vertebrate spindle elongation and cytokinesis. PLoS One. 2007; 2:e409. [PubMed: 17476331]

Burkard ME, Maciejowski J, Rodriguez-Bravo V, Repka M, Lowery DM, Clauser KR, Zhang C, Shokat KM, Carr SA, Yaffe MB, et al. Plk1 self-organization and priming phosphorylation of HsCYK-4 at the spindle midzone regulate the onset of division in human cells. PLoS Biol. 2009; 7:e1000111. [PubMed: 19468302]

Burkard ME, Randall CL, Larochelle S, Zhang C, Shokat KM, Fisher RP, Jallepalli PV. Chemical genetics reveals the requirement for Polo-like kinase 1 activity in positioning RhoA and triggering cytokinesis in human cells. Proc Natl Acad Sci U S A. 2007; 104:4383–4388. [PubMed: 17360533]

Canman JC, Lewellyn L, Laband K, Smerdon SJ, Desai A, Bowerman B, Oegema K. Inhibition of Rac by the GAP activity of centralspindlin is essential for cytokinesis. Science. 2008; 322:1543–1546. [PubMed: 19056985]

Chalamalasetty RB, Hummer S, Nigg EA, Sillje HH. Influence of human Ect2 depletion and overexpression on cleavage furrow formation and abscission. J Cell Sci. 2006; 119:3008–3019. [PubMed: 16803869]

Chang JH, Gill S, Settleman J, Parsons SJ. c-Src regulates the simultaneous rearrangement of actin cytoskeleton, p190RhoGAP, and p120RasGAP following epidermal growth factor stimulation. J Cell Biol. 1995; 130:355–368. [PubMed: 7542246]

Chang YC, Nalbant P, Birkenfeld J, Chang ZF, Bokoch GM. GEF-H1 couples nocodazole-induced microtubule disassembly to cell contractility via RhoA. Mol Biol Cell. 2008; 19:2147–2153. [PubMed: 18287519]

Cheeseman IM, Desai A. A combined approach for the localization and tandem affinity purification of protein complexes from metazoans. Sci STKE. 2005; 2005:pI1.

Chen W, Foss M, Tseng KF, Zhang D. Redundant mechanisms recruit actin into the contractile ring in silkworm spermatocytes. PLoS biology. 2008; 6:e209. [PubMed: 18767903]

D'Avino PP, Savoian MS, Glover DM. Mutations in sticky lead to defective organization of the contractile ring during cytokinesis and are enhanced by Rho and suppressed by Rac. J Cell Biol. 2004; 166:61–71. [PubMed: 15240570]

D'Avino PP, Savoian MS, Glover DM. Cleavage furrow formation and ingression during animal cytokinesis: a microtubule legacy. J Cell Sci. 2005; 118:1549–1558. [PubMed: 15811947]

Desai A, Rybina S, Muller-Reichert T, Shevchenko A, Shevchenko A, Hyman A, Oegema K. KNL-1 directs assembly of the microtubule-binding interface of the kinetochore in C. elegans. Genes Dev. 2003; 17:2421–2435. [PubMed: 14522947]

Desai A, Verma S, Mitchison TJ, Walczak CE. Kin I kinesins are microtubule-destabilizing enzymes. Cell. 1999; 96:69–78. [PubMed: 9989498]

Fededa JP, Gerlich DW. Molecular control of animal cell cytokinesis. Nat Cell Biol. 2012; 14:440–447. [PubMed: 22552143]

Fincham VJ, Chudleigh A, Frame MC. Regulation of p190 Rho-GAP by v-Src is linked to cytoskeletal disruption during transformation. J Cell Sci. 1999; 112(Pt 6):947–956. [PubMed: 10036244]

Foe VE, von Dassow G. Stable and dynamic microtubules coordinately shape the myosin activation zone during cytokinetic furrow formation. J Cell Biol. 2008; 183:457–470. [PubMed: 18955555]

Frenette P, Haines E, Loloyan M, Kinal M, Pakarian P, Piekny A. An anillin-Ect2 complex stabilizes central spindle microtubules at the cortex during cytokinesis. PLoS One. 2012; 7:e34888. [PubMed: 22514687]

Frokjaer-Jensen C, Davis MW, Hopkins CE, Newman BJ, Thummel JM, Olesen SP, Grunnet M, Jorgensen EM. Single-copy insertion of transgenes in Caenorhabditis elegans. Nat Genet. 2008; 40:1375–1383. [PubMed: 18953339]

Gai M, Camera P, Dema A, Bianchi F, Berto G, Scarpa E, Germena G, Di Cunto F. Citron kinase controls abscission through RhoA and anillin. Mol Biol Cell. 2011; 22:3768–78. [PubMed: 21849473]

Gassmann R, Holland AJ, Varma D, Wan X, Civril F, Cleveland DW, Oegema K, Salmon ED, Desai A. Removal of Spindly from microtubule-attached kinetochores controls spindle checkpoint silencing in human cells. Genes Dev. 2010; 24:957–971. [PubMed: 20439434]

Goode BL, Eck MJ. Mechanism and function of formins in the control of actin assembly. Annu Rev Biochem. 2007; 76:593–627. [PubMed: 17373907]

Graham DL, Eccleston JF, Lowe PN. The conserved arginine in rho-GTPase-activating protein is essential for efficient catalysis but not for complex formation with Rho.GDP and aluminum fluoride. Biochemistry. 1999; 38:985–991. [PubMed: 9893994]

Green RA, Paluch E, Oegema K. Cytokinesis in Animal Cells. Annu Rev Cell Dev Biol. 2012

Hu CK, Coughlin M, Mitchison TJ. Midbody assembly and its regulation during cytokinesis. Mol Biol Cell. 2012; 23:1024–34. [PubMed: 22278743]

Jantsch-Plunger V, Gonczy P, Romano A, Schnabel H, Hamill D, Schnabel R, Hyman AA, Glotzer M. CYK-4: A Rho family gtpase activating protein (GAP) required for central spindle formation and cytokinesis. J Cell Biol. 2000; 149:1391–1404. [PubMed: 10871280]

Kamath RS, Fraser AG, Dong Y, Poulin G, Durbin R, Gotta M, Kanapin A, Le Bot N, Moreno S, Sohrmann M, et al. Systematic functional analysis of the Caenorhabditis elegans genome using RNAi. Nature. 2003; 421:231–237. [PubMed: 12529635]

Kawashima T, Hirose K, Satoh T, Kaneko A, Ikeda Y, Kaziro Y, Nosaka T, Kitamura T. MgcRacGAP is involved in the control of growth and differentiation of hematopoietic cells. Blood. 2000; 96:2116–2124. [PubMed: 10979956]

Leonard DA, Lin R, Cerione RA, Manor D. Biochemical studies of the mechanism of action of the Cdc42-GTPase-activating protein. J Biol Chem. 1998; 273:16210–16215. [PubMed: 9632678]

Loria A, Longhini KM, Glotzer M. The RhoGAP domain of CYK-4 has an essential role in RhoA activation. Curr Biol. 2012; 22:213–219. [PubMed: 22226748]

Matsumura F, Yamakita Y, Yamashiro S. Myosin light chain kinases and phosphatase in mitosis and cytokinesis. Arch Biochem Biophys. 2011; 510:76–82. [PubMed: 21396909]

Matthews HK, Delabre U, Rohn JL, Guck J, Kunda P, Baum B. Changes in Ect2 localization couple actomyosin-dependent cell shape changes to mitotic progression. Dev Cell. 2012; 23:371–83. [PubMed: 22898780]

Miller AL, Bement WM. Regulation of cytokinesis by Rho GTPase flux. Nat Cell Biol. 2009; 11:71–77. [PubMed: 19060892]

Minoshima Y, Kawashima T, Hirose K, Tonozuka Y, Kawajiri A, Bao YC, Deng X, Tatsuka M, Narumiya S, May WS Jr, et al. Phosphorylation by aurora B converts MgcRacGAP to a RhoGAP during cytokinesis. Dev Cell. 2003; 4:549–560. [PubMed: 12689593]

Murthy K, Wadsworth P. Dual role for microtubules in regulating cortical contractility during cytokinesis. J Cell Sci. 2008; 121:2350–2359. [PubMed: 18559890]

Nakahara H, Mueller SC, Nomizu M, Yamada Y, Yeh Y, Chen WT. Activation of beta1 integrin signaling stimulates tyrosine phosphorylation of p190RhoGAP and membrane-protrusive activities at invadopodia. J Biol Chem. 1998; 273:9–12. [PubMed: 9417037]

Oegema K, Desai A, Rybina S, Kirkham M, Hyman AA. Functional analysis of kinetochore assembly in Caenorhabditis elegans. J Cell Biol. 2001; 153:1209–1226. [PubMed: 11402065]

Petronczki M, Glotzer M, Kraut N, Peters JM. Polo-like kinase 1 triggers the initiation of cytokinesis in human cells by promoting recruitment of the RhoGEF Ect2 to the central spindle. Dev Cell. 2007; 12:713–725. [PubMed: 17488623]

Piekny A, Werner M, Glotzer M. Cytokinesis: welcome to the Rho zone. Trends Cell Biol. 2005; 15:651–658. [PubMed: 16243528]

Piekny AJ, Glotzer M. Anillin is a scaffold protein that links RhoA, actin, and myosin during cytokinesis. Curr Biol. 2008; 18:30–36. [PubMed: 18158243]

Poser I, Sarov M, Hutchins JR, Heriche JK, Toyoda Y, Pozniakovsky A, Weigl D, Nitzsche A, Hegemann B, Bird AW, et al. BAC TransgeneOmics: a high-throughput method for exploration of protein function in mammals. Nat Methods. 2008; 5:409–415. [PubMed: 18391959]

Rankin KE, Wordeman L. Long astral microtubules uncouple mitotic spindles from the cytokinetic furrow. J Cell Biol. 2010; 190:35–43. [PubMed: 20603328]

Rappaport R. Repeated furrow formation from a single mitotic apparatus in cylindrical sand dollar eggs. J Exp Zool. 1985; 234:167–171. [PubMed: 3989496]

Riley B, Williamson M, Collier D, Wilkie H, Makoff A. A 3-Mb map of a large Segmental duplication overlapping the alpha7-nicotinic acetylcholine receptor gene (CHRNA7) at human 15q13-q14. Genomics. 2002; 79:197–209. [PubMed: 11829490]

Rittinger K, Walker PA, Eccleston JF, Smerdon SJ, Gamblin SJ. Structure at 1.65 A of RhoA and its GTPase-activating protein in complex with a transition-state analogue. Nature. 1997; 389:758–762. [PubMed: 9338791]

Rossman KL, Der CJ, Sondek J. GEF means go: turning on RHO GTPases with guanine nucleotide-exchange factors. Nat Rev Mol Cell Biol. 2005; 6:167–180. [PubMed: 15688002]

Rual JF, Ceron J, Koreth J, Hao T, Nicot AS, Hirozane-Kishikawa T, Vandenhaute J, Orkin SH, Hill DE, van den Heuvel S, et al. Toward improving Caenorhabditis elegans phenome mapping with an ORFeome-based RNAi library. Genome Res. 2004; 14:2162–2168. [PubMed: 15489339]

Schmutz C, Stevens J, Spang A. Functions of the novel RhoGAP proteins RGA-3 and RGA-4 in the germ line and in the early embryo of C. elegans. Development. 2007; 134:3495–3505. [PubMed: 17728351]

Schonegg S, Constantinescu AT, Hoege C, Hyman AA. The Rho GTPase-activating proteins RGA-3 and RGA-4 are required to set the initial size of PAR domains in Caenorhabditis elegans one-cell embryos. Proc Natl Acad Sci U S A. 2007; 104:14976–14981. [PubMed: 17848508]

Sonnichsen B, Koski LB, Walsh A, Marschall P, Neumann B, Brehm M, Alleaume AM, Artelt J, Bettencourt P, Cassin E, et al. Full-genome RNAi profiling of early embryogenesis in Caenorhabditis elegans. Nature. 2005; 434:462–469. [PubMed: 15791247]

Steigemann P, Wurzenberger C, Schmitz MH, Held M, Guizetti J, Maar S, Gerlich DW. Aurora B-mediated abscission checkpoint protects against tetraploidization. Cell. 2009; 136:473–484. [PubMed: 19203582]

Straight AF, Cheung A, Limouze J, Chen I, Westwood NJ, Sellers JR, Mitchison TJ. Dissecting Temporal and Spatial Control of Cytokinesis with a Myosin II Inhibitor. Science. 2003; 299:1743–1747. [PubMed: 12637748]

Su L, Agati JM, Parsons SJ. p190RhoGAP is cell cycle regulated and affects cytokinesis. J Cell Biol. 2003; 163:571–582. [PubMed: 14610059]

Su L, Pertz O, Mikawa M, Hahn K, Parsons SJ. p190RhoGAP negatively regulates Rho activity at the cleavage furrow of mitotic cells. Exp Cell Res. 2009; 315:1347–1359. [PubMed: 19254711]

Su KC, Takaki T, Petronczki M. Targeting of the RhoGEF Ect2 to the equatorial membrane controls cleavage furrow formation during cytokinesis. Dev Cell. 2011; 21:1104–15. [PubMed: 22172673]

Tcherkezian J, Lamarche-Vane N. Current knowledge of the large RhoGAP family of proteins. Biol Cell. 2007; 99:67–86. [PubMed: 17222083]

Tighe A, Johnson VL, Taylor SS. Truncating APC mutations have dominant effects on proliferation, spindle checkpoint control, survival and chromosome stability. J Cell Sci. 2004; 117:6339–6353. [PubMed: 15561772]

Toure A, Dorseuil O, Morin L, Timmons P, Jegou B, Reibel L, Gacon G. MgcRacGAP, a new human GTPase-activating protein for Rac and Cdc42 similar to Drosophila rotundRacGAP gene product, is expressed in male germ cells. J Biol Chem. 1998; 273:6019–6023. [PubMed: 9497316]

von Dassow G. Concurrent cues for cytokinetic furrow induction in animal cells. Trends Cell Biol. 2009; 19:165–173. [PubMed: 19285868]

von Dassow G, Verbrugghe KJ, Miller AL, Sider JR, Bement WM. Action at a distance during cytokinesis. J Cell Biol. 2009; 187:831–845. [PubMed: 20008563]

Werner M, Munro E, Glotzer M. Astral signals spatially bias cortical myosin recruitment to break symmetry and promote cytokinesis. Curr Biol. 2007; 17:1286–1297. [PubMed: 17669650]

Wolfe BA, Takaki T, Petronczki M, Glotzer M. Polo-like kinase 1 directs assembly of the HsCyk-4 RhoGAP/Ect2 RhoGEF complex to initiate cleavage furrow formation. PLoS Biol. 2009; 7:e1000110. [PubMed: 19468300]

Yonemura S, Hirao-Minakuchi K, Nishimura Y. Rho localization in cells and tissues. Exp Cell Res. 2004; 295:300–314. [PubMed: 15093731]

Yuce O, Piekny A, Glotzer M. An ECT2-centralspindlin complex regulates the localization and function of RhoA. J Cell Biol. 2005; 170:571–582. [PubMed: 16103226]

Zhou M, Wang YL. Distinct pathways for the early recruitment of myosin II and actin to the cytokinetic furrow. Molecular biology of the cell. 2008; 19:318–326. [PubMed: 17959823]

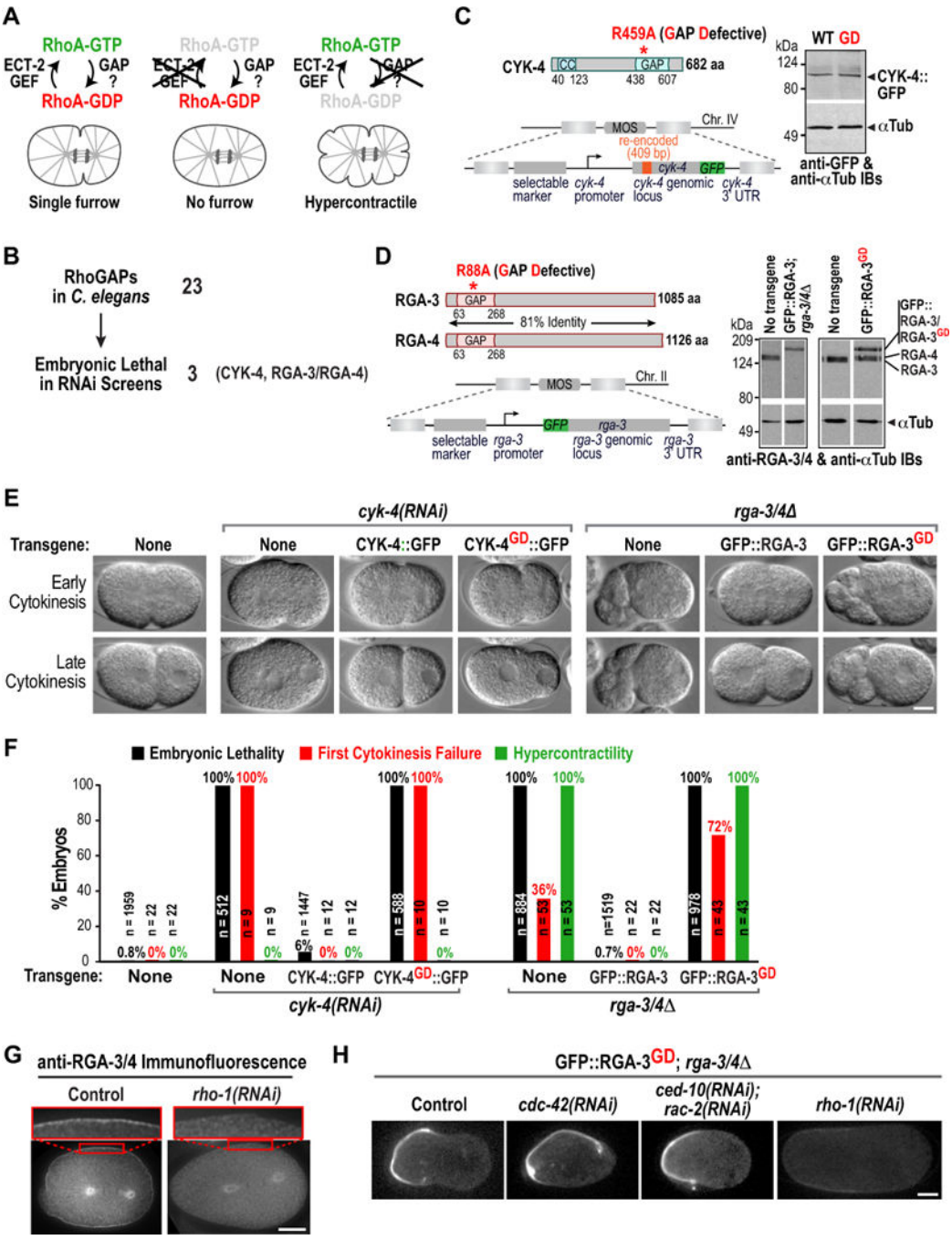


**Figure 1. The GAP Activity of RGA-3/4 restrains RhoA during mitosis and cytokinesis**

(**A**) Schematics of a wild-type embryo (***left***), an ECT-2 depleted embryo (***middle***); and of the predicted effect of inhibiting the RhoA GAP (***right***). (**B**) Of the 23 RhoGAPs in *C. elegans* only three (CYK-4, RGA-3, and RGA-4) are embryonic lethal (Table S1). (**C**) (***left***) Schematics of CYK-4 and the *cyk-4::gfp* transgene. (***right***) Immunoblot of worm extracts from the indicated transgenic strains probed for GFP and α-tubulin as a loading control. (**D**) (***left***) Schematics of RGA-3 and RGA-4 and of the *gfp::rga-3* transgene. (***right***) Immunoblot of worm extracts from N2 control and indicated transgenic strains; the strain expressing

GFP::RGA-3 was homozygous for *rga-3* and *rga-4* deletions (*rga-3/4Δ)*, whereas the strain expressing GFP::RGA-3$^{GD}$ was not. (**E**) DIC images during early and late cytokinesis for the indicated conditions. (**F**) Graph plotting embryonic lethality, first division cytokinesis failure, and hypercontractility (>2 ingressions during mitosis). n = number of embryos. (**G**) Immunofluorescence of one-cell stage wild-type (***left***) and *rho-1(RNAi)* (***right***) embryos stained with antibodies to RGA-3/4 (n>12 for each condition). (**H**) Central plane confocal images of one-cell stage metaphase *rga-3/4*Δ embryos expressing GFP-RGA-3$^{GD}$ after RNAi of the indicated genes (n>7 embryos for each condition). Bars, 10μm. See also Figure S1.

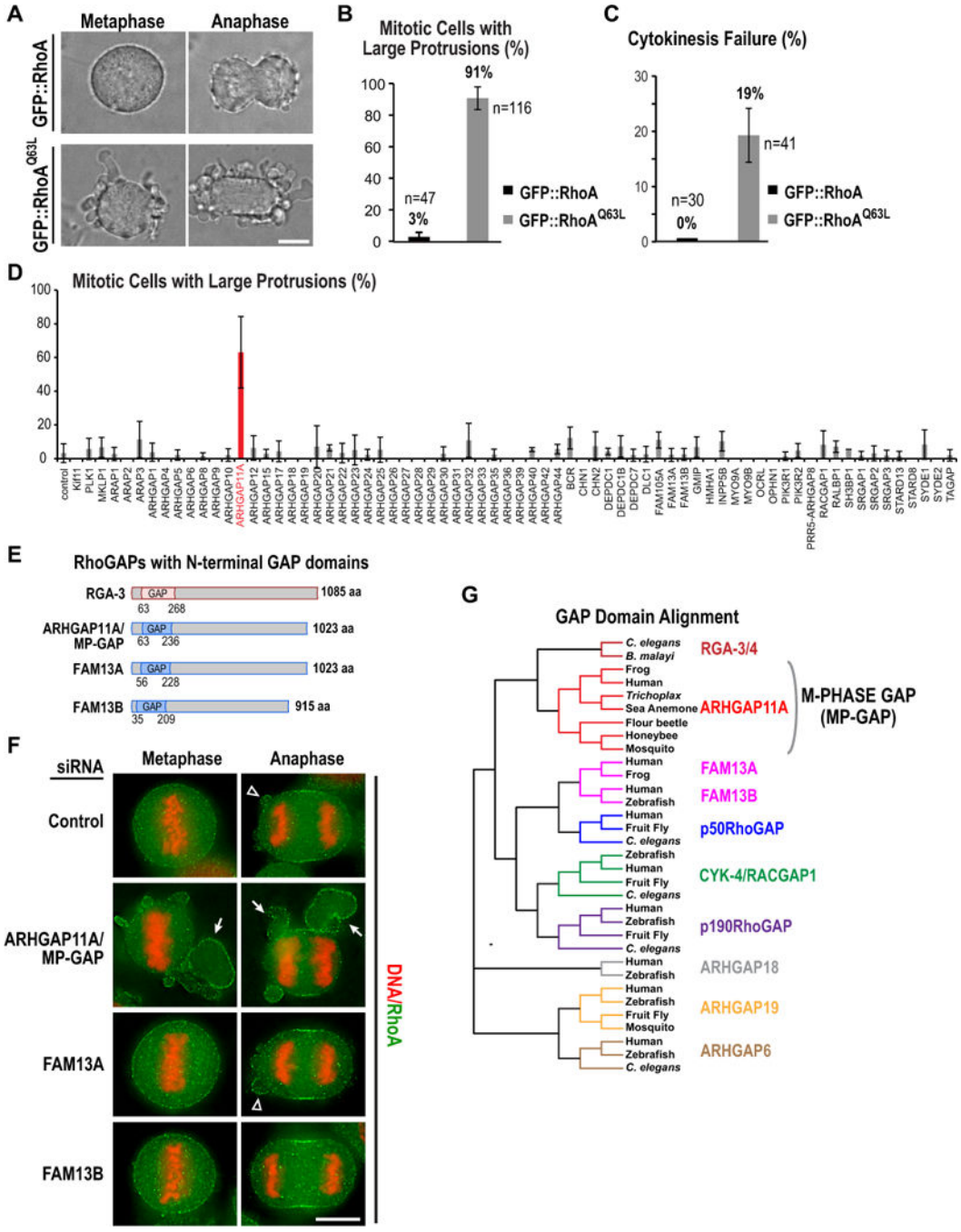


**Figure 2. Identification of a human GAP that opposes RhoA during mitosis**

(**A–C**) HeLa cells induced to express wild-type or constitutively active (Q63L) GFP::RhoA 16h prior to imaging. (**A**) Bright field images. (**B,C**) Graphs plotting the percentage of mitotic cells expressing each RhoA variant that have large protrusions (*B*) or exhibit cytokinesis failure (*C*). Error bars are SD from 2 or 3 independent experiments. n=total number of cells. (**D**) Graph plotting the mean percentage of mitotic cells with large protrusions across two (38 genes) or three (33 genes) independent experiments following knockdown of each of the predicted human RhoGAPs. Mitotic cells from all 4 siRNAs

targeting each gene were pooled. Error bars are SD. (**E**) Schematics of three human RhoGAPs with a domain architecture similar to *C. elegans* RGA-3. (**F**) Images of unsynchronized HeLa cells stained for DNA and RhoA after treatment with a control siRNA or pooled siRNAs targeting the indicated GAPs. Arrowheads point to small blebs, which are present in controls; arrows point to large protrusions resulting from ARHGAP11A knockdown. (**G**) Phylogenetic tree of a GAP domain alignment highlighting conservation of the MP-GAP family in invertebrates and primitive metazoans (for accession numbers see Fig. S2D). Bars in A and F, 10μm. See also Figure S2.

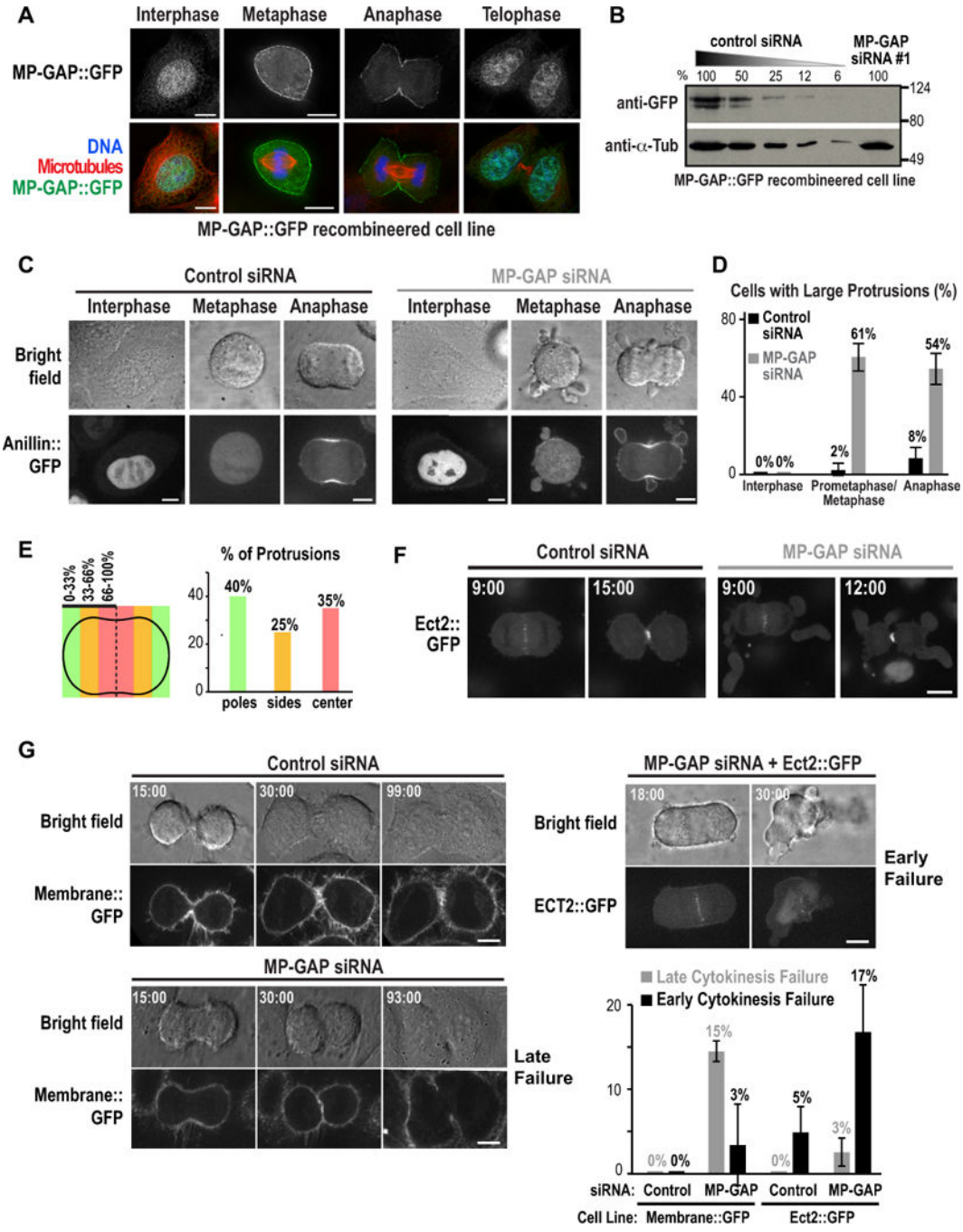


**Figure 3. MP-GAP controls cortical dynamics during mitosis and cytokinesis**

(**A**) HeLa cells expressing BAC-integrated MP-GAP::GFP fixed at different cell cycle stages and stained for DNA, GFP and microtubules. (**B**) Immunoblot of HeLa cells expressing BAC-integrated MP-GAP::GFP treated with MP-GAP siRNA#1 or a control siRNA for 48h. Serial dilutions of control cells were loaded to quantify depletion level. α-tubulin served as a loading control. (**C**) HeLa cells expressing BAC-integrated Anillin::GFP filmed starting 48 h after transfection with control or MP-GAP siRNA. Representative bright field (***top***) and confocal fluorescence (***bottom***) images are shown. (**D**) Graph of the

percentage of cells with large protrusions in interphase (n=2 experiments), prometaphase/metaphase (n=7 experiments), and anaphase (n=7 experiments). Error bars are the SD. Total number of cells analyzed: control siRNA (55 interphase, 245 prometaphase/metaphase, 263 anaphase), MP-GAP siRNA (55 interphase, 140 prometaphase/metaphase, 140 anaphase). (**E**) Graph showing the spatial distribution of protrusions in early anaphase fixed cells stained for RhoA and DNA. (40 protrusions from 2 independent experiments). (**F**) Fluorescence confocal images of HeLa cells expressing BAC-integrated Ect2::GFP 48h after transfection with control or MP-GAP siRNA. Times are minutes after anaphase onset. (**G**) Representative brightfield and confocal fluorescence images of the indicated conditions from timelapse imaging initiated ~8h after release from a thymidine block of HeLa cells expressing Membrane::GFP (MyrPalm:mEGFP) or Ect2::GFP. Times are minutes after anaphase onset. Graph shows percentage of early and late cytokinesis failure for each condition. Error bars are the SD of 2 (Membrane::GFP) or 3 (Ect2::GFP) independent experiments. The total number of cells analyzed was: Membrane::GFP (95 control siRNA, 90 MP-GAP siRNA); Ect2::GFP (179 control siRNA, 159 MP-GAP siRNA). Bars, 10μm. See also Figure S3.

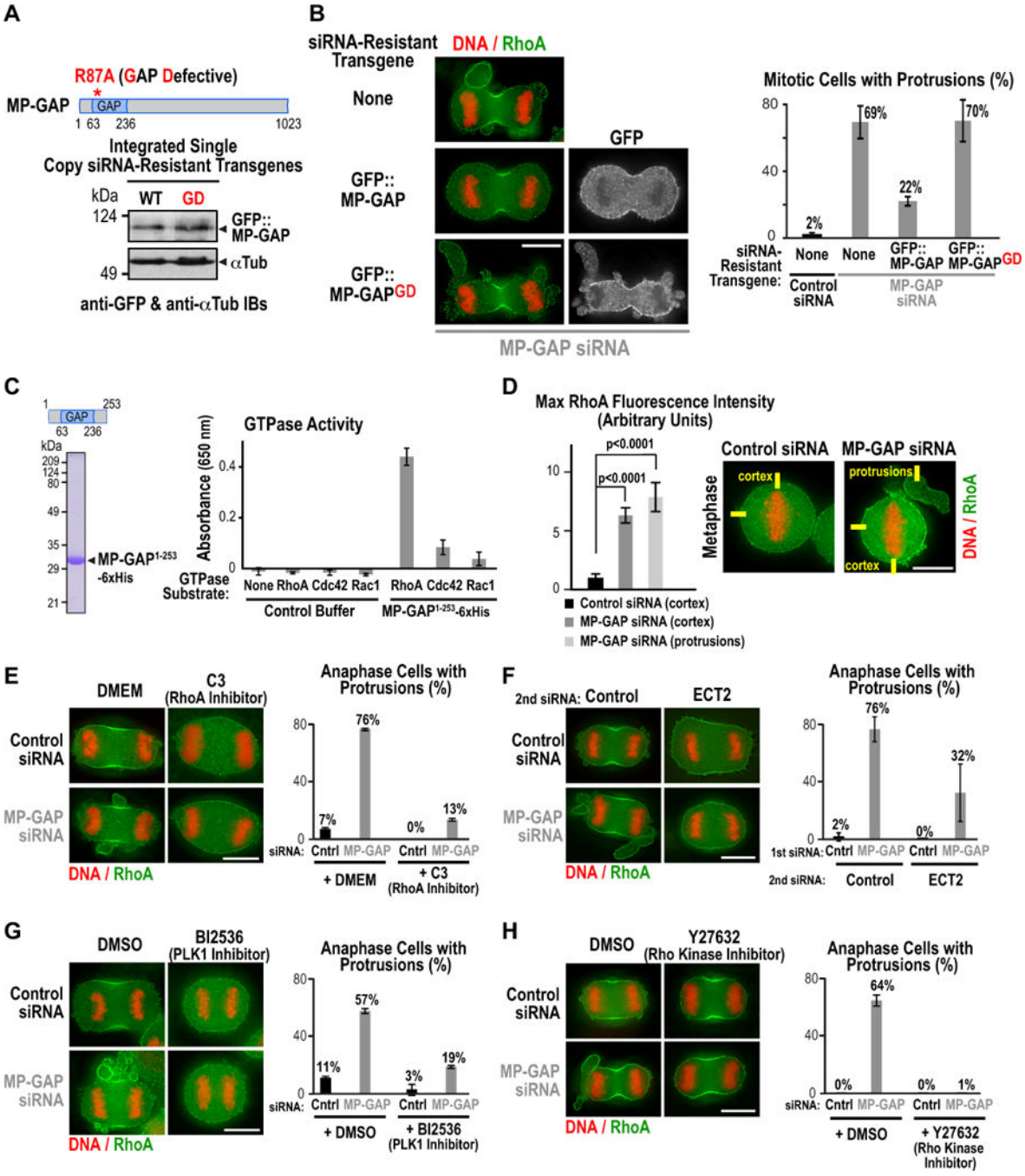


**Figure 4. MP-GAP suppresses cortical hypercontractility by targeting RhoA**

(**A**) Immunoblot of stable isogenic HeLa cell lines expressing GFP::MP-GAP or GAP-deficient GFP::MP-GAP$^{GD}$ probed with antibodies to GFP and α-tubulin. (**B**) (***left***) Immunofluorescence images of a control cell line or cell lines expressing GFP::MP-GAP or GFP::MP-GAP$^{GD}$ after transfection with MP-GAP siRNA. Cells were stained for DNA, RhoA and GFP. (***right***) Graph showing the mean percentage of mitotic cells with protrusions. Error bars are the SD of 3 independent experiments. Total number of cells analyzed: control siRNA (170 No transgene), MP-GAP siRNA (158 No transgene; 170

GFP::MP-GAP; 158 GFP::MP-GAP$^{GD}$). (**C**) (***left***) Coomassie-stained gel of purified GAP domain used in the *in vitro* GAP assay. (***right*)** Graph showing production of free phosphate, monitored by absorbance at 650 nm, after incubation of purified MP-GAP domain or control buffer with RhoA, Rac1 or Cdc42. Numbers are the mean from 3 independent experiments; error bars are the SD. (**D**) (***right***) Immunofluorescence images of synchronized HeLa cells treated with control or MP-GAP siRNA, arrested in metaphase with MG132, and fixed and stained for DNA and RhoA. (***left***) Graph of the maximum RhoA fluorescence intensity on the cell cortex (control and MP-GAP siRNA) or in the protrusions (MP-GAP siRNA) measured from 20 pixel wide linescans. The total number of linescans was: control siRNA (cortex, n=48), MP-GAP siRNA (cortex, n=64; protrusions, n=50). p-values are from student's t-tests. Error bars are the SEM. (**E–H**) Representative images of HeLa cells fixed and stained for DNA and RhoA. Graphs display the mean percentage of anaphase cells with protrusions. Error bars are the SD. Treatment protocols for each inhibitor/siRNA are outlined in Fig. S4A–E. (**E**) HeLa cells treated for 6 h with the RhoA inhibitor C3; the total number of analyzed cells in 2 independent experiments was control siRNA (30 DMEM; 37 C3), MP-GAP siRNA (49 DMEM; 46 C3). (**F**) HeLa cells transfected with control or MP-GAP siRNA for 24h followed by a second siRNA transfection (control or Ect2 siRNA) for 24h. The total number of analyzed cells in 3 independent experiments was: 1st siRNA control (2nd siRNA: 64 control; 67 Ect2); 1st siRNA MP-GAP (2nd siRNA: 69 control; 69 Ect2). (**G**) HeLa cells synchronized and treated with the PLK1 inhibitor BI2536 during anaphase. The total number of cells analyzed in 2 independent experiments was: control siRNA (114 DMSO; 84 BI2536), MP-GAP siRNA (130 DMSO; 151 BI2536). (**H**) HeLa cells treated for 1 h with the Rho kinase inhibitor Y27623. The total number of analyzed cells in 2 independent experiments was control siRNA (34 DMSO; 37 Y27623), MP-GAP siRNA (61 DMSO; 33 Y27623). Bars, 10μm. See also Figure S4.

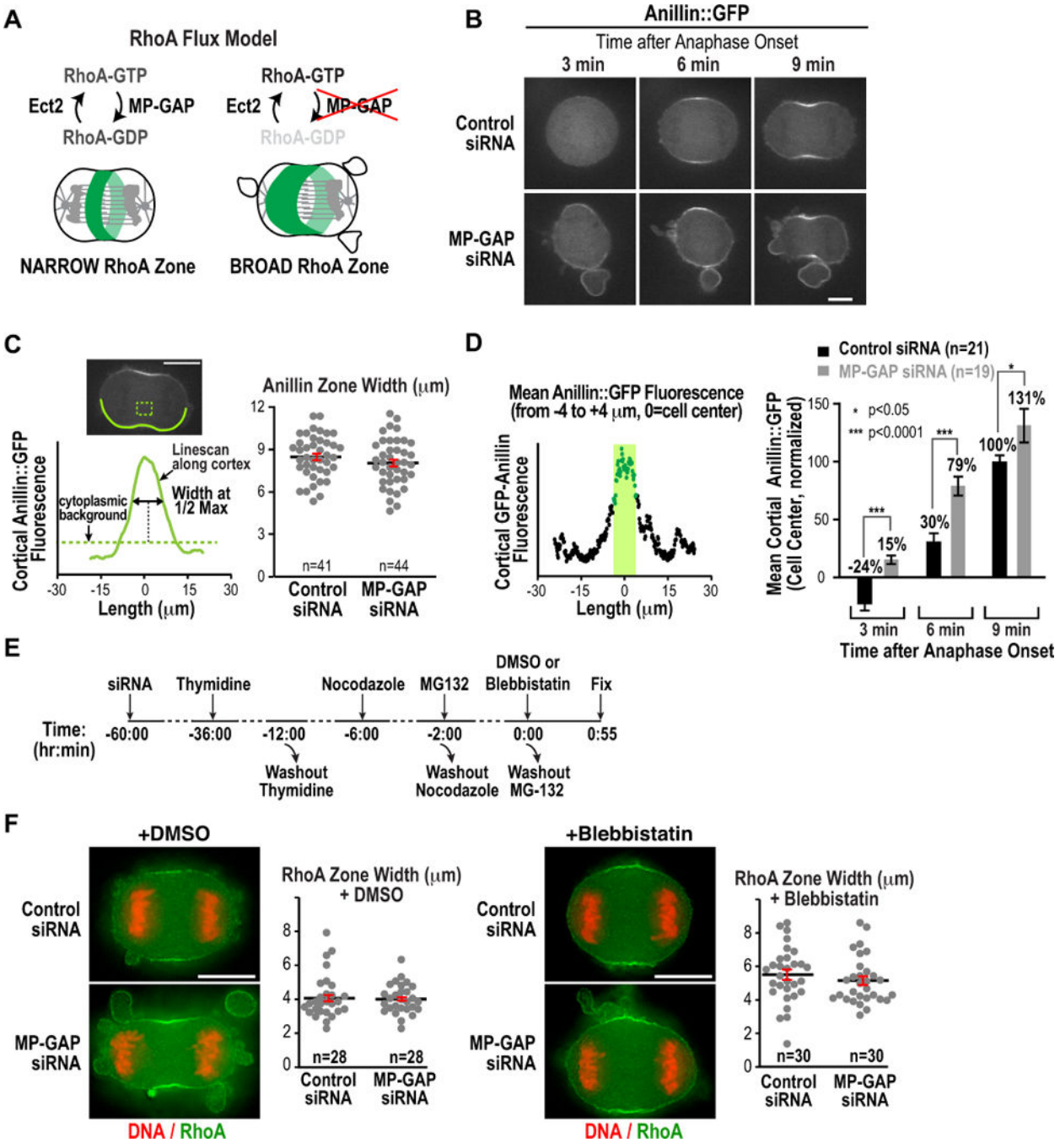


**Figure 5. MP-GAP inhibition accelerates RhoA accumulation but does not alter RhoA zone dimensions along the anaphase spindle**

(**A**) Schematic of the RhoA flux model. (**B**) Timelapse confocal fluorescence images of Anillin::GFP HeLa cells transfected with control or MP-GAP siRNA. (**C**) (***left***) Central plane confocal image and schematic illustrating the method used to measure the width of the Anillin::GFP zone. (***right***) Graph plotting the width of the Anillin::GFP zone in cells transfected with control or MP-GAP siRNA. Data from two independent experiments were pooled. n=number of linescans analyzed. Error bars are the SEM. (**D**) Mean Anillin::GFP

fluorescence intensity in an 8 μm wide equatorial region 3, 6 and 9 minutes after the last metaphase frame. Mean fluorescence intensities were measured from cortical linescans as described in *C* and were normalized to the mean intensity in controls at 9 minutes (set to 100%). Data from 2 independent experiments were pooled. The total number of cells analyzed was: control siRNA n=21, MP-GAP siRNA n=19. Error bars are the SEM. p-values are from student's t-tests. (**E**) Experimental scheme used to treat cells with blebbistatin at anaphase onset. (**F**) Width of the RhoA zone in fixed early anaphase DMSO and blebbistatin-treated cells measured as described in (*C*). n=number of linescans analyzed. Error bars are the SEM. Bars, 10 μm.

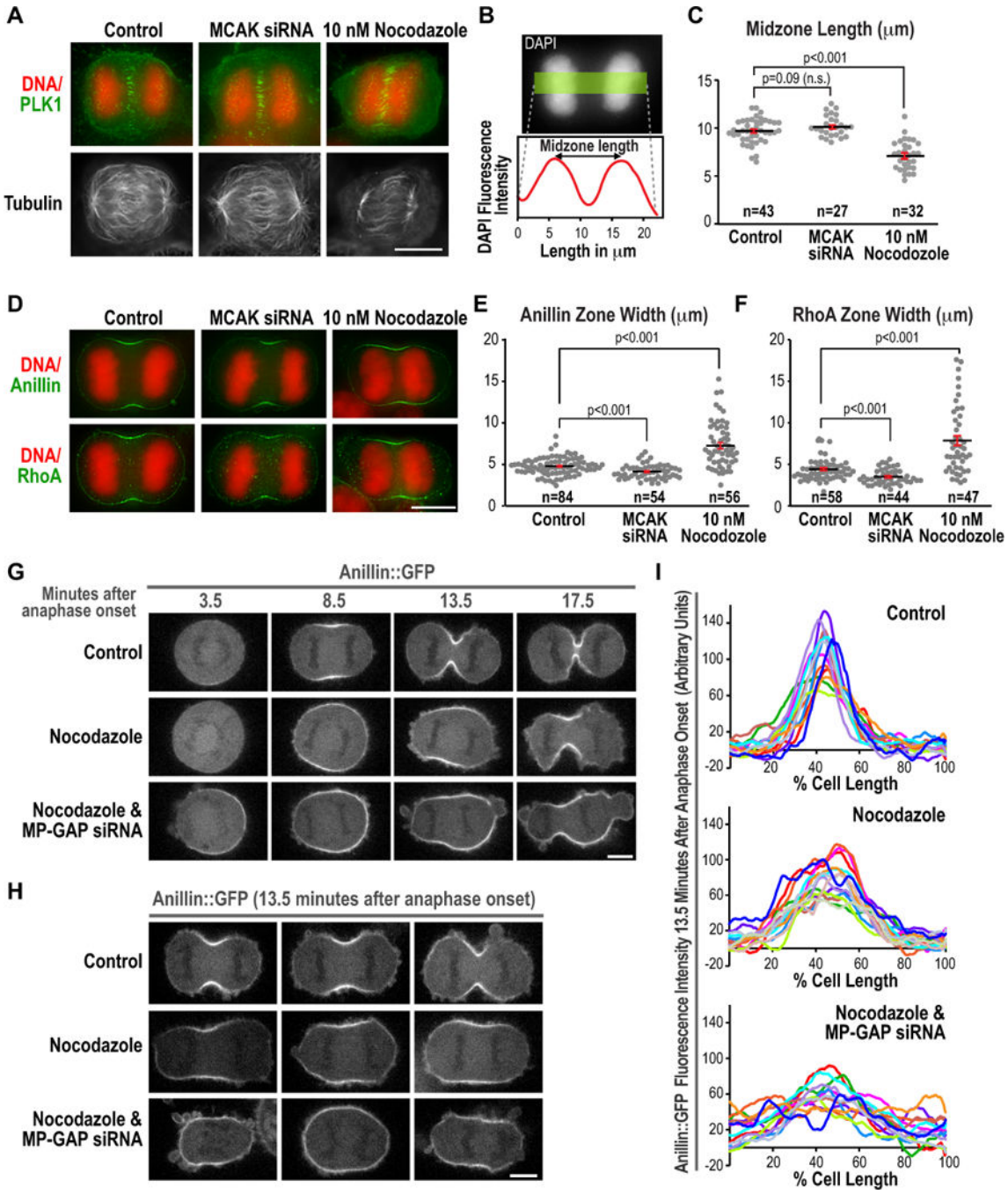


**Figure 6. MP-GAP mediated RhoA flux specifies RhoA zone dimensions when the centrosomal microtubule asters are absent**

(**A**) Immunofluorescence images of control, MCAK siRNA, and low dose nocodazole-treated cells stained for DNA, Plk1, and α-tubulin. (**B**) Measurement of midzone length from DNA fluorescence images of fixed early anaphase cells using a 50 pixel wide line scan and measuring the distance between the two peaks of DNA fluorescence intensity. (**C**) Graph of midzone length for control, MCAK siRNA-treated and low dose nocodazole-treated cells. n=number of cells scored. Error bars are the SEM. (**D**) Anaphase

immunofluorescence images of cells treated as indicated and stained for DNA and RhoA. (**E,F**) Graphs plotting the width of the Anillin zone (*E*) and the RhoA zone (*F*) measured as described in Fig. 5C. n= number of linescans analyzed. p-values are the student's t-test; error bars are the SEM. (**G–H**) Images of HeLa cells expressing Anillin::GFP. Representative timelapse sequences (*G*) or 3 images of cells ~13.5 minutes after anaphase onset (*H*) are shown for each condition. (**I**) Cortical Anillin::GFP fluorescence measured using a pole-to-pole linescan 13.5 minutes after anaphase onset. The average cortical fluorescence intensity at metaphase was subtracted from each value and the two linescans for each cell were averaged to generate each individual trace. Bars, 10 μm. See also Figure S5.

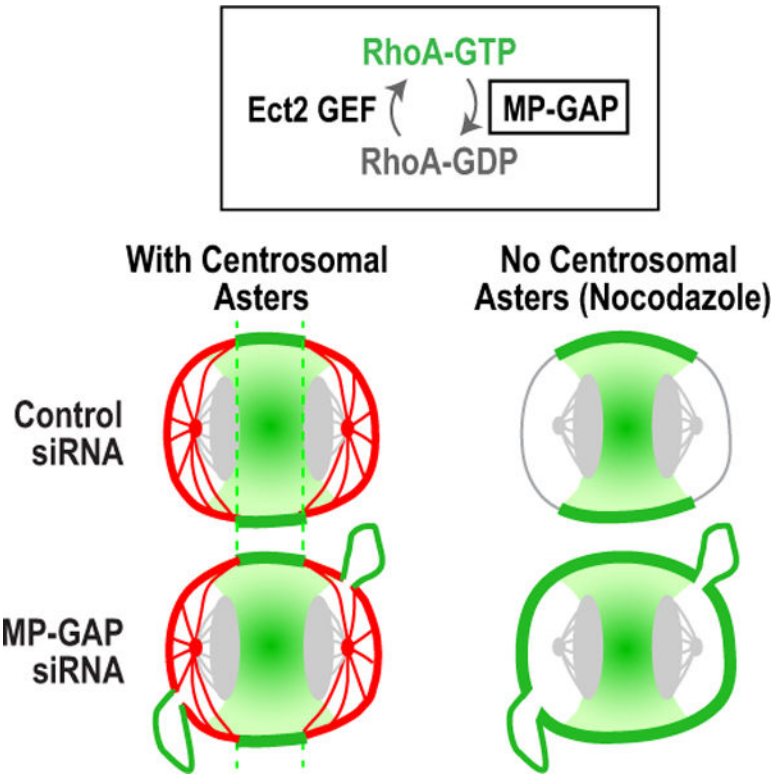


**Figure 7. MP-GAP controls RhoA zone formation in the absence of the centrosomal asters**

In control cells, RhoA zone dimensions are dominantly specified by the centrosomal asters. MP-GAP inhibition does not increase RhoA zone dimensions when the asters are present, but it does lead to the formation of large protrusions. In the absence of the centrosomal asters, MP-GAP inhibition broadens the equatorial RhoA zone indicating that RhoA zone dimensions are controlled by MP-GAP mediated RhoA flux.